

A PARTITIONED SCHEME FOR FLUID-STRUCTURE AND STRUCTURE-STRUCTURE INTERACTION WITH SLIP

Martina Bukač⁺, Sunčica Čanić^{*}, Boris Muha[#]

⁺*Applied and Computational Mathematics and Statistics, Notre Dame University, USA*

^{*}*Department of Mathematics, University of Houston, USA*

[#]*Department of Mathematics, Faculty of Science, University of Zagreb, Croatia*

1 BACKGROUND

In fluid mechanics the widely accepted boundary condition for viscous flows is the *no-slip* condition. When applied to fluid-structure interaction (FSI) problems this condition states that the fluid velocity at the moving boundary is equal to the velocity of the boundary itself. If the boundary is rigid and fixed, the no-slip condition states that the fluid velocity at the boundary is zero. This condition is justified only when molecular viscosity is considered. Requiring that the *normal component* of fluid velocity is zero at the boundary (the non-penetration condition) is reasonable (for impermeable solids):

$$(\partial_t \boldsymbol{\eta} - \mathbf{u}) \cdot \mathbf{n} = 0. \quad (1)$$

However, for the *tangential component* of fluid velocity Navier claimed that there should be a slip, and that the **slip velocity should be proportional to shear stress** [57]. For moving boundaries this conditions reads:

$$(\partial_t \boldsymbol{\eta} - \mathbf{u}) \cdot \boldsymbol{\tau} = \alpha \boldsymbol{\sigma} \mathbf{n} \cdot \boldsymbol{\tau}, \quad (2)$$

where $\partial_t \boldsymbol{\eta}$ is the fluid boundary (structure) velocity, \mathbf{u} is the fluid velocity at the boundary, $\boldsymbol{\sigma}$ is the fluid Cauchy stress tensor, $\boldsymbol{\tau}$ and \mathbf{n} are the tangent and normal vectors to the boundary, respectively, and α is the proportionality constant known as the slip length. Indeed, kinetic theory calculations have confirmed the Navier slip condition, but they gave the slip length proportional to the mean free path divided by the continuum length, which for practical purposes means zero slip length ($\alpha = 0$) justifying the use of no-slip condition.

Recent advances in technology, biomedical engineering, mathematical analysis and scientific computing have re-iterated the need for further studies involving the slip boundary condition. Indeed, recent studies have shown that the no-slip condition is not adequate to model contact between smooth rigid bodies immersed in an incompressible, viscous fluid since contact in such scenarios is **not possible** [64, 40, 41, 67]: A resolution to this **no-collision paradox** is to **employ a different boundary condition**, such as the Navier slip boundary condition, which allows contact between smooth rigid bodies [58]. Problems of this type arise, e.g., in modeling elastic heart valve closure, where different kinds of *ad hoc* “gap” conditions have been used to get around this difficulty [26].

By using the Navier slip boundary condition near the closure, a more realistic model of this FSI problem would be provided.

Another example where the Navier slip boundary condition is appropriate is the interaction between an incompressible, viscous fluid and elastic structures with “**rough**” **boundaries**. Such problems arise, e.g, in studying the interaction between blood flow and bio-artificial tissue constructs, which involve cells seeded on elastic tissue scaffolds with grooved microstructure. To filter out the small scales (small oscillations) of the rough fluid domain boundary, effective boundary conditions based on the Navier slip condition have been used in various application involving rigid boundaries [49, 50]. Instead of using the no-slip condition at the groove-scale, the Navier slip condition is applied at the corresponding “groove-free” *smooth* boundary [49, 50].

Other examples where the slip boundary condition should be used to accurately approximate the physics of the problem include the flow of water over **hydrophobic surfaces** (e.g., spray fabricated liquid repellent surfaces [68]), where it is known that there is an especially large slip at the fluid-solid interface. As an example we show in Figure 1 (left) a “classical” Ketchup flow, and in the middle panel we show the Ketchup flow in a bottle that had been treated with a no-stick coating. The two snap-shots were taken at the same time after the bottled had been tilted downwards. One can see significant difference in the flow characteristics. The panel on the right shows our numerical simulation of the Ketchup flow with the Navier-slip boundary condition, using a methodology based on Smooth Particle Hydrodynamics.



FIGURE 1: Hydrophilic vs. hydrophobic surfaces: no-slip vs. slip condition. Left: Classical Ketchup flow. Middle: Ketchup flowing in a bottle treated with a no-stick coating. Right: Our numerical simulation of flow with slip boundary condition. The pictures were taken at the same moment in time after the bottle throat started pointing downward.

In addition to considering the Navier slip as a boundary condition for fluid flows, various slip conditions have also been considered to model composite structures that experience sliding between different layers [38, 39, 6]. It has been shown that laminated beams [39] and multi-layered plates with *slip at the interface* between two layers [38, 6] provide structural damping in the oscillations of the composite, laminated structure. To the best of our knowledge, no studies of the interaction between such laminated structures and the flow of an incompressible, viscous fluid have been performed. Studying the interaction between these laminated materials with fluids is important in many

applications including, e.g., the stability of oil rigs [70] and in cardiovascular science. In cardiovascular science, for example, it is well known that arterial walls are composite structures consisting of several layers, each with different mechanical characteristic and thickness. Recent experimental studies performed by Cinthio et al. [20, 21, 1] report that in high adrenaline situations caused by emotional stress, the steep pressure wave fronts generated by the heart cause a significant shear strain between different layers of arterial walls. It was pointed out in [1] that the role of this phenomenon in atherogenesis is completely unexplored. To study this problem a model that describes vascular wall as a laminated structure with interfacial slip should be used.

The current mathematical literature on FSI with slip concerns studies involving rigid bodies [58, 32, 33, 17, 55, 63, 69]. To the best of our knowledge, there have been no general existence results or partitioned computational schemes for problems describing FSI between an incompressible, viscous fluid and an elastic solid satisfying the Navier slip boundary condition. The main mathematical difficulties stem from the fact that in FSI problems with slip the regularizing effects by the viscous fluid dissipation are no longer transmitted to the structure through the continuity of fluid and structure velocities, as is the case with the no-slip condition. This partial loss of information in the interaction between the fluid and structure is the main source of difficulties in the analysis and numerical method development for this class of problems. New compactness arguments need to be designed to study existence and well-posedness, and new ideas are needed to design a class of stable partitioned numerical schemes for this class of problems.

A recent work by Muha and Čanić [56] sheds light on the existence of weak solutions to fluid-structure interaction problems between incompressible, viscous fluids and linearly elastic shells or plates interacting via the Navier slip boundary condition. The existence proof is constructive: a sequence of approximate solutions to the coupled problem is obtained by semi-discretizing the problem in time via the Lie operator splitting strategy, as we explain below in Sec. 4. At every time step a fluid and a structure sub-problems are “solved” with boundary conditions that reflect two-way coupling between the fluid and structure, which includes the Navier slip boundary condition. This sequence of approximate solutions is then shown to converge to a weak solution to the coupled problem by designing clever compactness arguments.

Motivated by the main steps in this existence proof [56] in the present manuscript we propose a partitioned numerical scheme that can be used to solve fluid-structure interaction problems where the coupling between the fluid and structure incorporates the Navier slip boundary condition, and, additionally, the structure is composed of several layers, which are coupled through a slip condition. The fluid is modeled by the Navier-Stokes equations for an incompressible, viscous fluid, and two classes of structure models are considered. They include the equations of 3D or 2D elasticity, and reduced structure models such as the linearly and nonlinearly elastic membrane and Koiter shell equations. The fluid and structure, as well as the thin and thick structure, are coupled via two coupling conditions: the kinematic coupling condition describing slip in the tangential velocity components together with the non-penetration condition,

and the dynamics coupling condition describing balance of forces at the fluid-structure and structure-structure interface, see Sec. 3.

To solve this problem numerically, we propose here a partitioned, loosely coupled scheme. Partitioned schemes separate between different physics in the problem and allow the re-use of the already available computational solvers for the solution of the corresponding sub-problems. In this work the fluid and structure sub-problems are separated in a way so that the resulting scheme is unconditionally stable with just one calculation of the fluid and structure sub-problems at every time step. This avoids the expensive sub-iterations associated with the classical partitioned schemes such as the Dirichlet-Neumann schemes. Our simulations and uniform energy estimates support the claim of unconditional stability even when the fluid and structure have comparable densities, which is known to be a critical regime for the instabilities due to the *added mass effect* [15]. The coupling via the Navier slip condition introduces additional challenges in the design of such schemes. This is because in FSI problems with slip the regularizing effects by the viscous fluid dissipation are no longer transmitted to the structure directly through the continuity of fluid and structure velocities, as is the case with the no-slip condition. This partial loss of information due to the jump in the tangential components of velocities is the main source of difficulties in the analysis and numerical method development for this class of problems. Based on the knowledge gained from our recent existence result for an FSI problem with the Navier slip condition [56] we introduce here a partitioned, loosely coupled scheme that gets around these difficulties by separating the fluid from structure sub-problems using the time-discretization via Lie operator splitting, where the splitting is performed in such a way that: (1) the semi-discretized energy approximates well the continuous energy of the coupled problem, thereby getting around the difficulties associated with the added mass effect, and (2) the viscous dissipation due to slip is cleverly distributed between the fluid and structure sub-problems providing a tight coupling that compensates for the lack of direct smoothing by the fluid viscosity in the no-slip condition.

2 LITERATURE REVIEW AND STATE-OF-THE-ART

Classical FSI problems between an incompressible, viscous fluid and an elastic structure assuming the no-slip boundary condition have been extensively studied since the 1980's (see e.g. [4, 5, 45, 7, 47, 48, 23, 43, 66, 16, 35, 61, 62, 28, 36, 37, 25, 42, 65, 2, 44, 22, 31, 13, 51] and the references therein). The state-of-the art in the well-posedness theory includes results on global existence of *weak solutions* for FSI problems with various elastic structures [35, 51, 52, 53], and local existence of *strong unique solutions* for various elastic structures immersed in a viscous, incompressible fluid [23, 24, 19, 18, 4, 5, 45, 43]. All the global existence results involving elastic structures hold until the structure(s) are about to "touch" each other, i.e., until a contact. In [64, 40, 41, 67] it was shown, however, that such a contact is not possible when *rigid balls* with smooth boundaries interact with an incompressible viscous fluid, indicating that the no-slip condition may

not be a good physical model for FSI dynamics near a contact. In 2010 Nestupa and Penel proved that if the no-slip boundary condition is replaced with the slip boundary condition, collision can occur between two rigid bodies [58]. This sparked recent activity in the area of existence results for FSI problem involving rigid solids and slip boundary conditions [32, 33, 17, 55, 63, 69]. In particular, Gerard-Varet and Hillairet considered a FSI problem involving a rigid solid immersed in an incompressible Navier-Stokes flow with the slip boundary condition, and proved the existence of a weak solution up to collision [32]. In a subsequent work [33] they proved that prescribing the slip boundary condition allows collision between the immersed solid and the boundary. The most recent work in this area is a *global* existence results for a weak solution permitting collision of a “smooth” rigid body with a “smooth” fluid domain boundary, proved in [17].

Recent results by Muha and Čanić address existence of weak solutions to fluid-structure interactions problems involving incompressible, viscous fluids interacting with elastic shells in 2D [56], incorporating the Navier slip boundary condition. The existence proof was based on a robust strategy recently developed by Muha and Čanić, published in the Arch. Rat. Mech. Anal. [51] and in the J. Diff. Eq. [53], where two types of FSI problems with elastic structures satisfying the *no-slip* boundary condition were considered. The techniques developed in [51, 53] were *constructive*, and based on an operator splitting approach (Lie operator splitting [34]), which was then extended to problems with the Navier slip condition, in [56].

This robust strategy for analyzing fluid-structure interaction problems using the time-discretization via operator splitting was then used in the design a family of novel partitioned, loosely coupled schemes for numerical solution of FSI problems with elastic structures and no-slip condition [10, 9, 11, 8]. The partitioned, loosely coupled scheme presented in [10] deals successfully with the instabilities associated with the added mass effect, and it was shown in [14, 12] that the scheme is unconditionally stable. The main ideas behind the scheme were based on the existence proof by Muha and Čanić [51].

Regarding the literature on the interaction between elastic structures with slip, we mention the results by Hansen et al. [38, 39], where control of laminated structures with slip was studied, and the engineering literature based on the works of Bears et al. see e.g. [6] and the references therein, discussing damping by laminated structures due to slip. Problems with slip between multi-layered structures have also been considered in biology to model cells, such as, e.g., in [59, 60, 60] where a multiscale model for red blood cell was proposed, in which the lipid bilayer and the cytoskeleton were considered as two distinct layers of shells with sliding-only interaction. Furthermore, bilayer membrane models with interlayer slide have been proposed to model a lipid membrane in [71, 3] and *interleaflet* sliding in lipidic bilayers was studied in [27].

In the current work we propose a partitioned numerical scheme for FSI problems between viscous, incompressible fluids and multi-layered structures, where the coupling across the fluid-structure interface, and between different layers in the multi-layered structures satisfies a slip condition. Our ideas related to the numerical method development are deeply rooted in the knowledge we gained from the mathematical analysis of

the underlying problem.

3 PROBLEM DEFINITION

We begin by describing a benchmark problem for the interaction between an incompressible, viscous fluid and an elastic composite structure consisting of two layers, allowing slip between the fluid and composite structure, and between the two structural layers. The flow of an incompressible, viscous fluid is modeled by the Navier-Stokes equations in a time-dependent domain $\Omega_F(t)$, see Fig. 2:

$$\text{FLUID : } \left. \begin{aligned} \rho_F(\partial_t \mathbf{u} + \mathbf{u} \cdot \nabla \mathbf{u}) &= \nabla \cdot \boldsymbol{\sigma}^F(\mathbf{u}, p), \\ \nabla \cdot \mathbf{u} &= 0, \end{aligned} \right\} \text{ in } \Omega_F(t), t \in (0, T), \quad (3)$$

where ρ_F denotes fluid density, \mathbf{u} is the fluid velocity, $\boldsymbol{\sigma}^F$ is the fluid Cauchy stress tensor, $\boldsymbol{\sigma}^F = -p\mathbf{I} + 2\mu_F\mathbf{D}(\mathbf{u})$ for Newtonian fluids, p is the fluid pressure, μ is the kinematic viscosity coefficient, and $\mathbf{D}(\mathbf{u}) = \frac{1}{2}(\nabla \mathbf{u} + \nabla^T \mathbf{u})$ is the symmetrized gradient of fluid velocity \mathbf{u} .

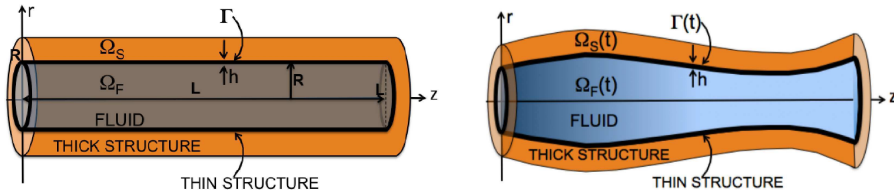


FIGURE 2: Example of fluid and structure domains.

To simplify presentation, we assume that the reference fluid domain is a cylinder of radius R and length L , denoted by Ω_F , with the lateral boundary denoted by Γ . We assume that the cylinder wall is compliant and that it consists of two layers: a thin layer, whose location at time t is denoted by $\Gamma(t)$, and a thick structural layer, whose location at time t is denoted by $\Omega_S(t)$, as shown in Figure 2.

We explain the main ideas for the case when the thin structure is modeled as a linearly elastic membrane or shell, described by the following general equations:

$$\text{THIN STRUCTURE : } \rho_S h \partial_{tt} \boldsymbol{\eta} + \mathcal{L}_e \boldsymbol{\eta} = \mathbf{f}, \quad \text{on } \Gamma, t \in (0, T), \quad (4)$$

where $\boldsymbol{\eta}$ is a vector function describing the displacement of the membrane/shell from its reference configuration Γ , \mathcal{L}_e is a coercive and continuous differential operator on the function space specified later, derived from the elastic energy of the thin structure, \mathbf{f} is force density (load), and ρ_S and h are the structure density and thickness, respectively.

The elastodynamics of the thick structural layer will be governed by the equations of linear elasticity. In Lagrangian coordinates, they describe the displacement \mathbf{d} of the

thick elastic structure with respect to a fixed, reference configuration Ω_S :

$$\text{THICK STRUCTURE: } \rho_T \partial_{tt} \mathbf{d} = \nabla \cdot \boldsymbol{\sigma}^S(\mathbf{d}) \text{ in } \Omega_S, t \in (0, T). \quad (5)$$

Here $\boldsymbol{\sigma}^S(\mathbf{d})$ is the first Piola-Kirchhoff stress tensor given by $\boldsymbol{\sigma}^S(\mathbf{d}) = 2\mu_S \mathbf{D}(\mathbf{d}) + \lambda_S (\nabla \cdot \mathbf{d}) \mathbf{I}$ for a linearly elastic material, and ρ_T is the thick structure density. Coefficients μ_S and λ_S are the Lamé constants describing the material properties of the structure.

The fluid, the thin structure and the thick structure are coupled via two sets of coupling conditions: the dynamic and kinematic coupling conditions. Denote by $\boldsymbol{\xi}$ the thin structure velocity, $\boldsymbol{\xi} = \partial_t \boldsymbol{\eta}$, and by \mathbf{v} the thick structure velocity, $\mathbf{v} = \partial_t \mathbf{d}$. The coupling we consider in this work is given by:

- DYNAMIC COUPLING CONDITION:

$$\rho_S h \partial_t \boldsymbol{\xi} + \mathcal{L}_e \boldsymbol{\eta} = -J \boldsymbol{\sigma}^F \mathbf{n}^F |_{\Gamma(t)} - \boldsymbol{\sigma}^S \mathbf{n}^S, \quad \text{on } \Gamma \times (0, T), \quad (6)$$

stating that the thin structure elastodynamics is driven by the jump in the normal stress across the interface. The term J is the Jacobian of the transformation between the Eulerian and Lagrangian formulations of the fluid and structure problems, respectively.

- KINEMATIC COUPLING CONDITION (including the Navier slip condition):

$$\begin{aligned} \boldsymbol{\xi} \cdot \mathbf{n}^F &= \mathbf{u} \cdot \mathbf{n}^F |_{\Gamma(t)} \text{ on } \Gamma \times (0, T) \quad (\text{the non-penetration condition}) \\ \boldsymbol{\eta} \cdot \mathbf{n}^S &= \mathbf{d} \cdot \mathbf{n}^S \text{ on } \Gamma \times (0, T) \quad (\text{continuity of normal displacement}) \\ (\boldsymbol{\xi} - \mathbf{u}) \cdot \boldsymbol{\tau}^F &= \alpha^{fs} J \boldsymbol{\sigma}^F \mathbf{n}^F \cdot \boldsymbol{\tau}^F |_{\Gamma(t)} \text{ on } \Gamma \times (0, T) \quad (\text{slip between fluid and structure}) \\ (\boldsymbol{\xi} - \mathbf{v}) \cdot \boldsymbol{\tau}^S &= \alpha^{ss} \boldsymbol{\sigma}^S \mathbf{n}^S \cdot \boldsymbol{\tau}^S \text{ on } \Gamma \times (0, T) \quad (\text{slip between structures}) \end{aligned}$$

Here, \mathbf{n} and $\boldsymbol{\tau}$ denote the outward normal and tangential unit vectors to the structure (superscript S) and fluid (superscript F) domains. This problem is supplemented with initial and boundary data defined on the portion of the boundary that is fixed, e.g., on the inflow and outflow boundaries shown in Fig. 2.

3.1 ENERGY ESTIMATE

One can show that the following formal energy inequality holds for this problem:

$$\begin{aligned} \frac{1}{2} \frac{d}{dt} \left(\rho_F \|\mathbf{u}\|_{L^2(\Omega^F(t))}^2 + \rho_S h \|\partial_t \boldsymbol{\eta}\|_{L^2(\Gamma)}^2 + \rho_T \|\partial_t \mathbf{d}\|_{L^2(\Omega^S)}^2 + c \|\boldsymbol{\eta}\|_{H^2(\Gamma)}^2 + 2\mu_S \|\mathbf{D}(\mathbf{d})\|_{L^2(\Omega^S)}^2 \right. \\ \left. + \lambda_S \|\nabla \cdot \mathbf{d}\|_{L^2(\Omega^S)}^2 + \mu_F \|\mathbf{D}(\mathbf{u})\|_{L^2(\Omega^F(t))}^2 + \frac{1}{\alpha^{fs}} \|u_\tau - \xi_\tau\|_{L^2(\Gamma)}^2 + \frac{1}{\alpha^{ss}} \|\xi_\tau - v_\tau\|_{L^2(\Gamma)}^2 \right) \leq \mathbf{C}, \end{aligned} \quad (7)$$

where the subscript τ denotes the tangential component of the vector function. In this estimate \mathbf{C} depends on the initial and boundary data, and constant c in front of the H^2 -norm of $\boldsymbol{\eta}$ is associated with the coercivity of the structure operator \mathcal{L}_e . This energy estimate shows that the proposed model is reasonable in the sense that the total kinetic and elastic energy of the coupled problem, plus dissipation due to fluid viscosity and slip friction are all bounded by a constant depending only on the initial and boundary data.

3.2 THE ALE FRAMEWORK

To deal with the difficulty associated with the fact that the fluid domain changes in time, we adopt the Arbitrary Lagrangian Eulerian (ALE) framework [42, 25]. The ALE approach is based on introducing a family of arbitrary, smooth, homeomorphic mappings \mathcal{A}_t defined on the reference domain Ω^F such that, for each $t \in (t_0, T)$, \mathcal{A}_t maps the reference domain Ω^F into the current domain $\Omega^F(t)$:

$$\mathcal{A}_t : \Omega^F \rightarrow \Omega^F(t) \subset \mathbb{R}^n, n = 2, 3, \quad \mathbf{x} = \mathcal{A}_t(\hat{\mathbf{x}}) \in \Omega^F(t), \quad \text{for } \hat{\mathbf{x}} \in \Omega^F.$$

Written in ALE framework, system (5) reads as follows: Find \mathbf{u} and p , with $\hat{\mathbf{u}}(\hat{\mathbf{x}}, t) = \mathbf{u}(\mathcal{A}_t(\hat{\mathbf{x}}), t)$ such that

$$\rho_F \left(\frac{\partial \mathbf{u}}{\partial t} \Big|_{\hat{\mathbf{x}}} + (\mathbf{u} - \mathbf{w}) \cdot \nabla \mathbf{u} \right) = \nabla \cdot \boldsymbol{\sigma}^F(\mathbf{u}, p), \quad \text{in } \Omega^F(t) \times (0, T), \quad (8)$$

$$\nabla \cdot \mathbf{u} = 0 \quad \text{in } \Omega^F(t) \times (0, T), \quad (9)$$

where

$$\mathbf{w} = \frac{\partial \mathcal{A}_t(\hat{\mathbf{x}})}{\partial t} \quad (10)$$

denotes the domain velocity. Note that $\frac{\partial f}{\partial t} \Big|_{\hat{\mathbf{x}}}$ denotes the time derivative of f evaluated on the reference domain.

4 NUMERICAL SCHEME

Our goal is to design a stable, partitioned scheme, which would separate the fluid from the composite structure, and at every time step require only *one solution* of the fluid and structure sub-problems, avoiding expensive sub-iterations typically associated with Dirichlet-Neumann partitioned FSI schemes [46]. Schemes that require only one sub-iteration between sub-problems at every time step are called *loosely coupled*.

There are many different ways the coupled FSI problem can be split into a fluid and a structure sub-problems. Our strategy is to semi-discretize our coupled evolution problem in time using the Lie operator splitting scheme [34]. The scheme is applied to our coupled problem which can be written, in general terms, as an evolution problem

$$\frac{dU}{dt} = AU = (A_1 + A_2)U, \quad t \in (0, T), \quad \text{with } U(0) = U_0.$$

The time interval is divided into N sub-intervals, and at every sub-interval (t_n, t_{n+1}) the coupled problem is semi-discretized in time and solved by splitting the problem into two sub-problems, defined by the operators A_1 and A_2 , following the Lie-Trotter formula [34]. More precisely, the sub-problem determined by the operator A_1 is solved ($dU/dt = A_1U$) with the initial data given by the solution from the previous time step,

i.e., the solution at $t = t_n$. Then, the sub-problem determined by the operator A_2 is solved ($dU/dt = A_2U$) over (t_n, t_{n+1}) with the initial data given by the just calculated solution of the sub-problem A_1 . Using this approach our coupled problem is split into two sub-problems, the fluid and structure sub-problems, which communicate via the initial data. To obtain a stable scheme, the trick is to perform the splitting, i.e., to define the operators A_1 and A_2 in such a way that the semi-discretized energy of the split problem approximates well the energy of the continuous problem. Based on our recent experience with partitioned schemes [51, 53, 54], we propose to split the dynamic coupling condition (6) into two parts, one serving as a boundary condition for the fluid sub-problem, and the other in the structure sub-problem, such that both parts include the time-derivative term (as defined by the Lie splitting):

$$\underbrace{\rho_S h \partial_t \xi}_{\text{fluid}} + \underbrace{\mathcal{L}_e \eta}_{\text{structure}} = \underbrace{-J \sigma^F n^F}_{\text{fluid}} - \underbrace{\sigma^S n^S}_{\text{structure}} \quad \text{on } \Gamma. \quad (11)$$

Here we note that n^F and n^S are outward normals to the fluid and thick structure domains, respectively, i.e., they point in opposite directions.

Although the Lie splitting scheme is generally first-order accurate in time, it has been shown that direct application of Lie scheme to FSI problems results in sub-optimal accuracy [12]. To increase the accuracy, we modify the Lie splitting in such a way that the structure “feels” the fluid not only via the initial data, but also through the loading exerted by the fluid onto the structure, given by $J \sigma^F n^F$. For this purpose, we rewrite the dynamic coupling condition (11) by adding and subtracting the normal fluid stress obtained at the previous time step $J \sigma^F n^F$, and use one part in the fluid and the other in the structure sub-problem:

$$\underbrace{\rho_S h \partial_t \xi}_{\text{fluid}} + \underbrace{\mathcal{L}_e \eta}_{\text{structure}} = \underbrace{-J \sigma^F n^F}_{\text{fluid}} - \underbrace{\sigma^S n^S}_{\text{structure}} + \underbrace{J \sigma^F n^F}_{\text{fluid}} \underbrace{- J \sigma^F n^F}_{\text{structure}} \quad \text{on } \Gamma. \quad (12)$$

This way the structure sub-problem “feels” the fluid not only via the initial data but also via the newly added term $J \sigma^F n^F$.

Based on these ideas, we propose here the following scheme. First, on each time interval (t_n, t_{n+1}) a structure problem is solved for the thick structure, modeled by (13) below, with boundary conditions at the thin-thick structure interface incorporating the slip, the non-penetration condition and the dynamic coupling condition. This boundary condition is obtained from the “structure part” of the dynamic coupling condition (12):

$$\rho_S h \partial_t \xi + \mathcal{L}_e \eta = -\sigma^S n^S - J \sigma^F n^F \quad \text{on } \Gamma,$$

by first writing this condition in components: the tangential and normal component. Then, the non-penetration condition between the thin and thick structure is taken into

account in the normal direction, giving rise to (14), while in the tangential direction, the forcing by the fluid Cauchy stress onto the thin structure $J^n \boldsymbol{\sigma}^F(\mathbf{u}^n, p^n) \mathbf{n}^F \cdot \boldsymbol{\tau}^S$ is replaced by friction due to slip between the thin and thick structure: $-\frac{1}{\alpha^{fs}}(\boldsymbol{\xi}^{n+1} - \mathbf{u}^n) \cdot \boldsymbol{\tau}^S$, obtained from the Navier slip condition. Similarly, the forcing by the first Piola-Kirchoff stress coming from the thick structure acting on the thin structure is replaced by friction due to slip between the thin and thick structure, giving rise to (15). Thus, the elastodynamics of the thin fluid-structure interface in tangential direction is entirely driven by the jump in friction across the interface itself. The initial data for the thin structure velocity is given by $(\mathbf{u} \cdot \mathbf{n}^S, \boldsymbol{\xi} \cdot \boldsymbol{\tau}^S)$ obtained from the previous time step. This explains the derivation of the boundary conditions (14) and (15) below.

Next, a fluid sub-problem is solved for the Navier-Stokes equations defined on the fluid domain $\Omega(t^n)$, with a Robin-type boundary condition at the fluid-structure interface $\Gamma(t^n)$. The normal component of this Robin condition is given by the three fluid terms in (12):

$$\rho_{sh} \partial_t \boldsymbol{\xi} \cdot \mathbf{n}^F = -J \boldsymbol{\sigma}^F \mathbf{n}^F \cdot \mathbf{n}^F + (J \boldsymbol{\sigma}^F \mathbf{n}^F)^n \cdot \mathbf{n}^F, \quad \text{on } \Gamma,$$

where the acceleration term on the left hand-side is discretized in time $(\boldsymbol{\xi}^{n+1} - \boldsymbol{\xi}^n) \cdot \mathbf{n}^F / \Delta t$ and the term $\boldsymbol{\xi}^{n+1} \cdot \mathbf{n}^F$ is replaced by $\mathbf{u}^{n+1} \cdot \mathbf{n}^F$ due to the non-penetration condition, while the initial data term $\boldsymbol{\xi}^n \cdot \mathbf{n}^F$ is taken to be the just calculated velocity of the thin structure from the structure sub-problem, which we denoted by $\boldsymbol{\xi}^{n+1} \cdot \mathbf{n}^F$. The tangential component of the Robin condition for \mathbf{u}^{n+1} on $\Gamma(t^n)$ is determined from the Navier slip condition. This explains the derivation of condition (18) below.

After the fluid and structure sub-problems are calculated, the fluid domain is updated via an ALE mapping, as we specify below.

To present details of the scheme, we introduce the following notation for the first order discrete time derivative:

$$d_t \varphi^{n+1} := (\varphi^{n+1} - \varphi^n) / \Delta t.$$

STEP A1 (STRUCTURE). Given \mathbf{u}^n and p^n from the previous time step, calculate $\boldsymbol{\xi}^{n+1} \cdot \boldsymbol{\tau}$, \mathbf{d}^{n+1} and \mathbf{v}^{n+1} such that

$$\mathbf{v}^{n+1} = d_t \mathbf{d}^{n+1}, \boldsymbol{\xi}^{n+1} = d_t \boldsymbol{\eta}^{n+1}$$

and the thick structure equations hold:

$$\rho_T d_t \mathbf{v}^{n+1} = \nabla \cdot \boldsymbol{\sigma}^S(\mathbf{d}^{n+1}) \quad \text{in } \Omega^S \quad (13)$$

with the following boundary conditions at the thin-thick structure interface Γ

$$\rho_{sh} \frac{\mathbf{v}^{n+1} - \mathbf{u}^n}{\Delta t} \cdot \mathbf{n}^S + \mathcal{L}_e \mathbf{d}^{n+1} \cdot \mathbf{n}^S = -J^n \boldsymbol{\sigma}(\mathbf{u}^n, p^n) \mathbf{n}^F \cdot \mathbf{n}^S - \boldsymbol{\sigma}^S(\mathbf{d}^{n+1}) \mathbf{n}^S \cdot \mathbf{n}^S \quad (14)$$

$$\rho_{sh} \frac{\boldsymbol{\xi}^{n+1} - \boldsymbol{\xi}^n}{\Delta t} \cdot \boldsymbol{\tau}^S + \mathcal{L}_e \boldsymbol{\eta}^{n+1} \cdot \boldsymbol{\tau}^S = -\frac{1}{\alpha^{fs}} (\boldsymbol{\xi}^{n+1} - \mathbf{u}^n) \cdot \boldsymbol{\tau}^S - \frac{1}{\alpha^{ss}} (\boldsymbol{\xi}^{n+1} - \mathbf{v}^{n+1}) \cdot \boldsymbol{\tau}^S \quad (15)$$

$$(\boldsymbol{\xi}^{n+1} - \mathbf{v}^{n+1}) \cdot \boldsymbol{\tau}^S = \alpha^{ss} \boldsymbol{\sigma}^S(\mathbf{d}^{n+1}) \mathbf{n}^S \cdot \boldsymbol{\tau}^S$$

From here we can calculate the thin structure displacement via

$$\boldsymbol{\eta}^{n+1} \cdot \mathbf{n}^S = \mathbf{d}^{n+1} \cdot \mathbf{n}^S, \quad \boldsymbol{\eta}^{n+1} \cdot \boldsymbol{\tau}^S = \Delta t \boldsymbol{\xi}^{n+1} \cdot \boldsymbol{\tau}^S + \boldsymbol{\eta}^n \cdot \boldsymbol{\tau}^S.$$

STEP A2 (FLUID). Given the thin structure location $\boldsymbol{\eta}^{n+1}$ and velocity $\boldsymbol{\xi}^{n+1}$, calculate $(\mathbf{u}^{n+1}, p^{n+1})$ such that:

$$\left. \begin{aligned} \rho_F d_t \mathbf{u}^{n+1}|_{\Omega^F} + \rho_F ((\mathbf{u}^n - \mathbf{w}^n) \cdot \nabla) \mathbf{u}^{n+1} &= \nabla \cdot \boldsymbol{\sigma}(\mathbf{u}^{n+1}, p^{n+1}) \\ \nabla \cdot \mathbf{u}^{n+1} &= 0 \end{aligned} \right\} \text{ in } \Omega^F(t^n) \quad (16)$$

with the following boundary data at the fluid-structure interface $\Gamma(t^n)$:

$$\begin{aligned} \rho_S h \frac{\mathbf{u}^{n+1} - \boldsymbol{\xi}^{n+1}}{\Delta t} \cdot \mathbf{n}^F + J^n \boldsymbol{\sigma}(\mathbf{u}^{n+1}, p^{n+1}) \mathbf{n}^F \cdot \mathbf{n}^F &= J^n \boldsymbol{\sigma}(\mathbf{u}^n, p^n) \mathbf{n}^F \cdot \mathbf{n}^F, \\ \mathbf{u}^{n+1} \cdot \boldsymbol{\tau}^F + \alpha^{fs} J^n \boldsymbol{\sigma}(\mathbf{u}^{n+1}, p^{n+1}) \mathbf{n}^F \cdot \boldsymbol{\tau}^F &= \boldsymbol{\xi}^{n+1} \cdot \boldsymbol{\tau}^F. \end{aligned} \quad (17)$$

FLUID DOMAIN UPDATE. Given the displacement $\boldsymbol{\eta}^{n+1}$ of the boundary Γ , we update the fluid domain $\Omega^F(t^{n+1})$ in a classical way by using the harmonic extension $\text{Ext}(\boldsymbol{\eta}^{n+1})$ of the boundary data $\boldsymbol{\eta}^{n+1}$ onto the entire domain, and compute the ALE velocity \mathbf{w}^{n+1} which is defined as the time derivative of the ALE mapping. More precisely, calculate the ALE mapping as:

$$\mathcal{A}_{t^{n+1}}(\hat{\mathbf{x}}) = \hat{\mathbf{x}} + \text{Ext}(\boldsymbol{\eta}^{n+1}) \quad \forall \hat{\mathbf{x}} \in \Omega^F,$$

and update

$$\Omega^F(t^{n+1}) = \mathcal{A}_{t^{n+1}}(\Omega^F), \quad \mathbf{w}^{n+1} = \frac{d\mathcal{A}_{t^{n+1}}}{dt} = \frac{\mathbf{x}^{n+1} - \mathbf{x}^n}{\Delta t}, \quad (19)$$

where $\mathbf{x}^{n+1} = \mathcal{A}_{t^{n+1}}^{-1}(\hat{\mathbf{x}}) \in \Omega^F(t^{n+1})$ and $\mathbf{x}^n = \mathcal{A}_{t^n}^{-1}(\hat{\mathbf{x}}) \in \Omega^F(t^n)$, for $\hat{\mathbf{x}} \in \Omega^F$.

SET $n = n + 1$ AND RETURN TO STEP A1.

Remark 1. We remark that in this scheme the kinematic coupling condition describing continuity of the normal components of the velocity between the fluid and thin structure is satisfied asynchronously, and not identically. It is, in general, not true in this scheme that $\mathbf{u}^n \cdot \mathbf{n}^F = \boldsymbol{\xi}^n \cdot \mathbf{n}^F$. Only in the limit as $\Delta t \rightarrow 0$, this will be satisfied. In fact, we show below that this condition is satisfied to the second-order accuracy in Δt .

Remark 2. We further remark that the splitting proposed here is slightly different from the splitting discussed in the existence proof in [56], and it is significantly different from the splitting schemes proposed by the authors in [10, 51] to solve FSI problems with the no-slip kinematic coupling condition. One important difference is the form of the Robin boundary condition for the fluid sub-problem. In contrast with the earlier

works [10, 51, 9, 11, 8, 56], the Robin boundary condition (17), (18) ties the fluid and structure inertia implicitly *only* in the normal component of the inertia. The lack of implicit coupling between the fluid and structure inertia in loosely coupled schemes for problems with no-slip condition typically leads to instabilities due to the added mass effect. We show below that this is not the case here. Our energy estimate for the semi-discretized problem, presented in (38) and (39) below, shows that the energy of the semi-discretized problem is bounded, uniformly in Δt , indicating that this scheme is also unconditionally stable. This is interesting because it says that in FSI problems with slip, the normal and tangential components of the velocity do not play equal roles in the stability of numerical schemes. Normal displacement influences volume change and tangential displacement only “reshuffles” the points within the elastic structure. In the tangential direction dissipation due to slip friction is sufficient to provide stability of our scheme. This is new. It is because of friction due to slip that our scheme does not require implicit coupling between the fluid and structure inertia in both the normal and tangential direction, and still provides an unconditionally stable partitioned scheme without the need for sub-iterations at every time step.

4.1 FULLY DISCRETIZED SCHEME IN WEAK FORM

We discretize problem (13)-(19) in space using a finite element method approach. Let

$$V^F(t) = \{\varphi : \Omega^F(t) \rightarrow \mathbb{R}^d \mid \varphi = \hat{\varphi} \circ (\mathcal{A}_t)^{-1}, \hat{\varphi} \in (H^1(\Omega^F))^d\}, \quad (20)$$

$$Q(t) = \{\psi : \Omega^F(t) \rightarrow \mathbb{R} \mid \psi = \hat{\psi} \circ (\mathcal{A}_t)^{-1}, \hat{\psi} \in L^2(\Omega^F)\}, \quad (21)$$

$$V^T = \{\varphi \in (H^1(\Omega^S))^d \mid \varphi = 0 \text{ on } \Gamma_{in/out}^S\}, \quad (22)$$

$$V^S = \{\chi \in (H^1(\Gamma))^d \mid \chi = 0 \text{ at } x = 0, L\}, \quad (23)$$

for all $t \in [0, T]$, where d stands for the dimension of the problem. These are the spaces associated with the fluid, pressure, thick structure problem, and the thin structure problem.

We recall here that the thin structure operator \mathcal{L}_E , obtained from the elastic energy of the thin structure, is coercive and continuous on the space V^S , which defines a bilinear form on V^S :

$$a_E(\chi, \eta) = \int_{\Gamma} \mathcal{L}_E \chi \cdot \eta,$$

and the norm

$$\|\eta\|_E^2 := a_E(\eta, \eta). \quad (24)$$

We will use this norm in the energy estimate below.

The finite element spaces are then defined as the subspaces $V_h^f \subset V^f$, $Q_h \subset Q$, $V_h^T \subset V^T$ and $V_h^S \subset V^S$ based on a conforming finite element triangulation with maximum triangle diameter $h = \Delta x$. We assume that spaces V_h^f and Q_h^f are *inf-sup* stable. The main steps of the scheme are given as follows:

STEP A1 (STRUCTURE): Given \mathbf{u}_h^n and p_h^n from the previous time step, calculate $\boldsymbol{\xi}_h^{n+1} \cdot \boldsymbol{\tau}$, \mathbf{d}_h^{n+1} and \mathbf{v}_h^{n+1} such that

$$\mathbf{v}_h^{n+1} = d_t \mathbf{d}_h^{n+1}, \boldsymbol{\xi}_h^{n+1} = d_t \boldsymbol{\eta}_h^{n+1}$$

and the following weak form of problem (13)-(15) holds for all $(\boldsymbol{\varphi}_h^S, \boldsymbol{\chi}_h) \in V_h^T \times V_h^S$:

$$\begin{aligned} & \rho_T \int_{\Omega^S} d_t \mathbf{v}_h^{n+1} \cdot \boldsymbol{\varphi}_h^S + 2\mu_S \int_{\Omega^S} \mathbf{D}(\mathbf{d}_h^{n+1}) : \mathbf{D}(\boldsymbol{\varphi}_h^S) + \lambda_S \int_{\Omega^S} (\nabla \cdot \mathbf{d}_h^{n+1})(\nabla \cdot \boldsymbol{\varphi}_h^S) \\ & + \frac{\rho_S h}{\Delta t} \int_{\Gamma} (\mathbf{v}_h^{n+1} \cdot \mathbf{n}^S)(\boldsymbol{\varphi}_h^S \cdot \mathbf{n}^S) + \rho_S h \int_{\Gamma} (d_t \boldsymbol{\xi}_h^{n+1} \cdot \boldsymbol{\tau}^S)(\boldsymbol{\chi}_h \cdot \boldsymbol{\tau}^S) + \int_{\Gamma} (\mathcal{L}_e \mathbf{d}_h^{n+1} \cdot \mathbf{n}^S)(\boldsymbol{\varphi}_h^S \cdot \mathbf{n}^S) \\ & \quad + \int_{\Gamma} (\mathcal{L}_e \boldsymbol{\eta}_h^{n+1} \cdot \boldsymbol{\tau}^S)(\boldsymbol{\chi}_h \cdot \boldsymbol{\tau}^S) + \frac{1}{\alpha^{ss}} \int_{\Gamma} (\mathbf{v}_h^{n+1} - \boldsymbol{\xi}_h^{n+1}) \cdot \boldsymbol{\tau}^S (\boldsymbol{\varphi}_h^S - \boldsymbol{\chi}_h) \cdot \boldsymbol{\tau}^S \\ & + \frac{1}{\alpha^{fs}} \int_{\Gamma} (\boldsymbol{\xi}_h^{n+1} \cdot \boldsymbol{\tau}^S)(\boldsymbol{\chi}_h \cdot \boldsymbol{\tau}^S) = \frac{\rho_S h}{\Delta t} \int_{\Gamma} (\mathbf{u}_h^n \cdot \mathbf{n}^S)(\boldsymbol{\varphi}_h^S \cdot \mathbf{n}^S) + \frac{1}{\alpha^{fs}} \int_{\Gamma} (\mathbf{u}_h^n \cdot \boldsymbol{\tau}^S)(\boldsymbol{\chi}_h \cdot \boldsymbol{\tau}^S) \\ & \quad - \int_{\Gamma} J^n (\boldsymbol{\sigma}(\mathbf{u}_h^n, p_h^n) \mathbf{n}^F|_{\Gamma} \cdot \mathbf{n}^S)(\boldsymbol{\varphi}_h^S \cdot \mathbf{n}^S) \end{aligned} \quad (25)$$

STEP A2 (FLUID): Given the thin structure location $\boldsymbol{\eta}_h^{n+1}$ and velocity $\boldsymbol{\xi}_h^{n+1}$, calculate $(\mathbf{u}_h^{n+1}, p_h^{n+1})$ such that for all $(\boldsymbol{\varphi}_h^F, \psi_h) \in V_h^F \times Q_h$

$$\begin{aligned} & \rho_F \int_{\Omega^F(t^n)} d_t \mathbf{u}_h^{n+1} \cdot \boldsymbol{\varphi}_h^F + \rho_F \int_{\Omega^F(t^n)} ((\mathbf{u}_h^n - \mathbf{w}_h^n) \cdot \nabla) \mathbf{u}_h^{n+1} \cdot \boldsymbol{\varphi}_h^F \\ & + 2\mu_F \int_{\Omega^F(t^n)} \mathbf{D}(\mathbf{u}_h^{n+1}) : \mathbf{D}(\boldsymbol{\varphi}_h^F) - \int_{\Omega^F(t^n)} p_h^{n+1} \nabla \cdot \boldsymbol{\varphi}_h^F + \int_{\Omega^F(t^n)} \psi \nabla \cdot \mathbf{u}_h^{n+1} \\ & \quad + \frac{1}{\alpha^{fs}} \int_{\Gamma} (\mathbf{u}_h^{n+1} \cdot \boldsymbol{\tau}^F)(\boldsymbol{\varphi}_h^F \cdot \boldsymbol{\tau}^F) + \frac{\rho_S h}{\Delta t} \int_{\Gamma} (\mathbf{u}_h^{n+1} \cdot \mathbf{n}^F)(\boldsymbol{\varphi}_h^F \cdot \mathbf{n}^F) \\ & \quad = \frac{1}{\alpha^{fs}} \int_{\Gamma} (\boldsymbol{\xi}_h^{n+1} \cdot \boldsymbol{\tau}^F)(\boldsymbol{\varphi}_h^F \cdot \boldsymbol{\tau}^F) + \frac{\rho_S h}{\Delta t} \int_{\Gamma} (\boldsymbol{\xi}_h^{n+1} \cdot \mathbf{n}^F)(\boldsymbol{\varphi}_h^F \cdot \mathbf{n}^F) \\ & \quad + \int_{\Gamma} J^n (\boldsymbol{\sigma}(\mathbf{u}_h^n, p_h^n) \mathbf{n}^F|_{\Gamma} \cdot \mathbf{n}^F)(\boldsymbol{\varphi}_h^F \cdot \mathbf{n}^F) - \int_{\Gamma_{in/out}} p_{in/out}(t^n) \boldsymbol{\varphi}_h^F \cdot \mathbf{n}^F dx. \end{aligned} \quad (26)$$

4.2 STABILITY ENERGY ESTIMATE

The main goal is to show that the splitting scheme (25), (26) is designed in such a way that the energy of the discretized problem approximates well the energy of the continuous problem. To simplify calculations and focus on the issues related to the splitting strategy, we introduce the following simplifying assumptions:

- Fluid domain is fixed (i.e., geometric nonlinearities are neglected).
- Fluid advection is neglected.

These two issues are related since energy estimates for the problem with advection must include moving domain in order to control the cubic terms that arise in the corresponding energy [51, 56]. These simplifying assumptions are normally used in stability analysis of FSI partitioned schemes [12, 29, 30].

We first derive an energy equality with the assumption that the pressure driving the problem is zero, and then obtain an energy inequality assuming that the inlet and outlet pressure are not necessarily equal to zero.

We start by obtain the energy of the fluid and structure sub-problems by replacing the test functions in (25) by: $\varphi_h^S = \mathbf{v}_h^{n+1}$, $\chi_h = \boldsymbol{\xi}_h^{n+1}$, and the test function in (26) by: $\varphi_h^F = \mathbf{u}_h^{n+1}$, $\psi = p_h^{n+1}$. Adding the resulting equations together and multiplying by Δt one gets the following:

$$\begin{aligned}
& \frac{\rho_T}{2} \left(\|\mathbf{v}_h^{n+1}\|_{L^2(\Omega^S)}^2 - \|\mathbf{v}_h^n\|_{L^2(\Omega^S)}^2 + \|\mathbf{v}_h^{n+1} - \mathbf{v}_h^n\|_{L^2(\Omega^S)}^2 \right) \\
& + \mu_S \left(\|\mathbf{D}(\mathbf{d}_h^{n+1})\|_{L^2(\Omega^S)}^2 - \|\mathbf{D}(\mathbf{d}_h^n)\|_{L^2(\Omega^S)}^2 + \|\mathbf{D}(\mathbf{d}_h^{n+1} - \mathbf{d}_h^n)\|_{L^2(\Omega^S)}^2 \right) \\
& + \frac{\lambda_S}{2} \left(\|\nabla \cdot \mathbf{d}_h^{n+1}\|_{L^2(\Omega^S)}^2 - \|\nabla \cdot \mathbf{d}_h^n\|_{L^2(\Omega^S)}^2 + \|\nabla \cdot (\mathbf{d}_h^{n+1} - \mathbf{d}_h^n)\|_{L^2(\Omega^S)}^2 \right) \\
& + \frac{\rho_S h}{2} \left(\|\boldsymbol{\xi}_h^{n+1} \cdot \boldsymbol{\tau}^S\|_{L^2(\Gamma)}^2 - \|\boldsymbol{\xi}_h^n \cdot \boldsymbol{\tau}^S\|_{L^2(\Gamma)}^2 + \|(\boldsymbol{\xi}_h^{n+1} - \boldsymbol{\xi}_h^n) \cdot \boldsymbol{\tau}^S\|_{L^2(\Gamma)}^2 \right) \\
& + \frac{1}{2} \left(\|\boldsymbol{\eta}_h^{n+1}\|_E^2 - \|\boldsymbol{\eta}_h^n\|_E^2 + \|\boldsymbol{\eta}_h^{n+1} - \boldsymbol{\eta}_h^n\|_E^2 \right) + \frac{\Delta t}{\alpha^{SS}} \|(\mathbf{v}_h^{n+1} - \boldsymbol{\xi}_h^{n+1}) \cdot \boldsymbol{\tau}^S\|_{L^2(\Gamma)}^2 \\
& + \frac{\rho_S h}{2} \left(\|\boldsymbol{\xi}_h^{n+1} \cdot \mathbf{n}^S\|_{L^2(\Gamma)}^2 - \|\mathbf{u}_h^n \cdot \mathbf{n}^S\|_{L^2(\Gamma)}^2 + \|(\boldsymbol{\xi}_h^{n+1} - \mathbf{u}_h^n) \cdot \mathbf{n}^S\|_{L^2(\Gamma)}^2 \right) \\
& + \frac{\Delta t}{2\alpha^{FS}} \left(\|\boldsymbol{\xi}_h^{n+1} \cdot \boldsymbol{\tau}^S\|_{L^2(\Gamma)}^2 - \|\mathbf{u}_h^n \cdot \boldsymbol{\tau}^S\|_{L^2(\Gamma)}^2 + \|(\boldsymbol{\xi}_h^{n+1} - \mathbf{u}_h^n) \cdot \boldsymbol{\tau}^S\|_{L^2(\Gamma)}^2 \right) \\
& + \frac{\rho_F}{2} \left(\|\mathbf{u}_h^{n+1}\|_{L^2(\Omega^F)}^2 - \|\mathbf{u}_h^n\|_{L^2(\Omega^F)}^2 + \|\mathbf{u}_h^{n+1} - \mathbf{u}_h^n\|_{L^2(\Omega^F)}^2 \right) + 2\Delta t \mu_F \|\mathbf{D}(\mathbf{u}_h^{n+1})\|_{L^2(\Omega^F)}^2 \\
& + \frac{\rho_S h}{2} \left(\|\mathbf{u}_h^{n+1} \cdot \mathbf{n}^F\|_{L^2(\Gamma)}^2 - \|\boldsymbol{\xi}_h^{n+1} \cdot \mathbf{n}^F\|_{L^2(\Gamma)}^2 + \|(\mathbf{u}_h^{n+1} - \boldsymbol{\xi}_h^{n+1}) \cdot \mathbf{n}^F\|_{L^2(\Gamma)}^2 \right) \\
& + \frac{\Delta t}{2\alpha^{FS}} \left(\|\mathbf{u}_h^{n+1} \cdot \boldsymbol{\tau}^F\|_{L^2(\Gamma)}^2 - \|\boldsymbol{\xi}_h^{n+1} \cdot \boldsymbol{\tau}^F\|_{L^2(\Gamma)}^2 + \|(\mathbf{u}_h^{n+1} - \boldsymbol{\xi}_h^{n+1}) \cdot \boldsymbol{\tau}^F\|_{L^2(\Gamma)}^2 \right) \\
& = \Delta t \underbrace{\int_{\Gamma} J^n (\boldsymbol{\sigma}(\mathbf{u}_h^n, p_h^n) \mathbf{n}^F|_{\Gamma} \cdot \mathbf{n}^S) (\mathbf{u}_h^{n+1} \cdot \mathbf{n}^S - \mathbf{v}_h^{n+1} \cdot \mathbf{n}^S)}_{\mathcal{I}}. \tag{27}
\end{aligned}$$

To express the right hand-side in terms of the L^2 norms of the fluid and structure quantities we notice that (17) implies:

$$\mathbf{u}_h^{n+1} \cdot \mathbf{n}^S - \boldsymbol{\xi}_h^{n+1} \cdot \mathbf{n}^S = -\frac{\Delta t}{\rho_S h} J^n (\boldsymbol{\sigma}(\mathbf{u}_h^{n+1}, p_h^{n+1}) \mathbf{n}^F|_{\Gamma} - \boldsymbol{\sigma}(\mathbf{u}_h^n, p_h^n) \mathbf{n}^F|_{\Gamma}) \cdot \mathbf{n}^S \quad \text{on } \Gamma.$$

This is interesting not only because we will use this in the energy estimate, but also because it shows that the kinematic coupling condition in the normal direction (the non-penetration condition) is satisfied in our scheme to the second-order accuracy in Δt , namely:

$$\mathbf{u}_h^{n+1} \cdot \mathbf{n}^S = \boldsymbol{\xi}_h^{n+1} \cdot \mathbf{n}^S + \frac{(\Delta t)^2}{\rho_S h} d_t \boldsymbol{\sigma}(\mathbf{u}_h^n, p_h^n) \mathbf{n}^F|_{\Gamma} \cdot \mathbf{n}^S.$$

With this observation the integral \mathcal{I} on the right hand-side of (27) becomes:

$$\begin{aligned}
\mathcal{I} &= \int_{\Gamma} J^n (\boldsymbol{\sigma}(\mathbf{u}_h^n, p_h^n) \mathbf{n}^F |_{\Gamma} \cdot \mathbf{n}^S) (\mathbf{u}_h^{n+1} \cdot \mathbf{n}^S - \mathbf{v}_h^{n+1} \cdot \mathbf{n}^S) \\
&= \frac{\Delta t}{2\rho_S h} \|J^n \boldsymbol{\sigma}(\mathbf{u}^n, p^n) \mathbf{n}^F |_{\Gamma} \cdot \mathbf{n}^S\|_{L^2(\Gamma)}^2 - \frac{\Delta t}{2\rho_S h} \|J^n \boldsymbol{\sigma}(\mathbf{u}^{n+1}, p^{n+1}) \mathbf{n}^F |_{\Gamma} \cdot \mathbf{n}^S\|_{L^2(\Gamma)}^2 \\
&\quad + \frac{\Delta t}{2\rho_S h} \|J^n (\boldsymbol{\sigma}(\mathbf{u}^{n+1}, p^{n+1}) \mathbf{n}^F |_{\Gamma} - \boldsymbol{\sigma}(\mathbf{u}^n, p^n) \mathbf{n}^F |_{\Gamma}) \cdot \mathbf{n}^S\|_{L^2(\Gamma)}^2 \\
&= \frac{\Delta t}{2\rho_S h} \|J^n \boldsymbol{\sigma}(\mathbf{u}^n, p^n) \mathbf{n}^F |_{\Gamma} \cdot \mathbf{n}^S\|_{L^2(\Gamma)}^2 - \frac{\Delta t}{2\rho_S h} \|J^n \boldsymbol{\sigma}(\mathbf{u}^{n+1}, p^{n+1}) \mathbf{n}^F |_{\Gamma} \cdot \mathbf{n}^S\|_{L^2(\Gamma)}^2 \\
&\quad + \frac{\rho_S h}{2\Delta t} \|(\mathbf{u}^{n+1} - \mathbf{v}^{n+1}) \cdot \mathbf{n}^S\|_{L^2(\Gamma)}^2. \tag{28}
\end{aligned}$$

Now, the last term in (28) cancels out the same term on the left hand-side in (27) (where we recall that $\mathbf{v}^{n+1} \cdot \mathbf{n}^S = \boldsymbol{\xi}^{n+1} \cdot \mathbf{n}^S$), and we obtain the following energy equality:

$$\begin{aligned}
&\frac{\rho_T}{2} \left(\|\mathbf{v}_h^{n+1}\|_{L^2(\Omega^S)}^2 + \|\mathbf{v}_h^{n+1} - \mathbf{v}_h^n\|_{L^2(\Omega^S)}^2 \right) \\
&\quad + \mu_S \left(\|\mathbf{D}(\mathbf{d}_h^{n+1})\|_{L^2(\Omega^S)}^2 + \|\mathbf{D}(\mathbf{d}_h^{n+1} - \mathbf{d}_h^n)\|_{L^2(\Omega^S)}^2 \right) \\
&\quad + \frac{\lambda_S}{2} \left(\|\nabla \cdot \mathbf{d}_h^{n+1}\|_{L^2(\Omega^S)}^2 + \|\nabla \cdot (\mathbf{d}_h^{n+1} - \mathbf{d}_h^n)\|_{L^2(\Omega^S)}^2 \right) \\
&\quad + \frac{\rho_F}{2} \left(\|\mathbf{u}_h^{n+1}\|_{L^2(\Omega^F)}^2 + \|\mathbf{u}_h^{n+1} - \mathbf{u}_h^n\|_{L^2(\Omega^F)}^2 \right) + 2\Delta t \mu_F \|\mathbf{D}(\mathbf{u}_h^{n+1})\|_{L^2(\Omega^F)}^2 \\
&+ \frac{\rho_S h}{2} \left(\|\boldsymbol{\xi}_h^{n+1} \cdot \boldsymbol{\tau}^S\|_{L^2(\Gamma)}^2 + \|\mathbf{u}_h^{n+1} \cdot \mathbf{n}^F\|_{L^2(\Gamma)}^2 + \|(\boldsymbol{\xi}_h^{n+1} - \boldsymbol{\xi}_h^n) \cdot \boldsymbol{\tau}^S\|_{L^2(\Gamma)}^2 + \|(\boldsymbol{\xi}_h^{n+1} - \mathbf{u}_h^n) \cdot \mathbf{n}^S\|_{L^2(\Gamma)}^2 \right) \\
&\quad + \frac{1}{2} \left(\|\boldsymbol{\eta}_h^{n+1}\|_E^2 + \|\boldsymbol{\eta}_h^{n+1} - \boldsymbol{\eta}_h^n\|_E^2 \right) + \frac{\Delta t}{\alpha^s s} \|(\mathbf{v}_h^{n+1} - \boldsymbol{\xi}_h^{n+1}) \cdot \boldsymbol{\tau}^S\|_{L^2(\Gamma)}^2 \\
&\quad + \frac{\Delta t}{2\alpha^f s} \left(\|\mathbf{u}_h^{n+1} \cdot \boldsymbol{\tau}^F\|_{L^2(\Gamma)}^2 + \|(\boldsymbol{\xi}_h^{n+1} - \mathbf{u}_h^n) \cdot \boldsymbol{\tau}^S\|_{L^2(\Gamma)}^2 + \|(\mathbf{u}_h^{n+1} - \boldsymbol{\xi}_h^{n+1}) \cdot \boldsymbol{\tau}^F\|_{L^2(\Gamma)}^2 \right) \\
&\quad + \frac{(\Delta t)^2}{2\rho_S h} \|J^n \boldsymbol{\sigma}(\mathbf{u}^{n+1}, p^{n+1}) \mathbf{n}^F |_{\Gamma} \cdot \mathbf{n}^S\|_{L^2(\Gamma)}^2 \\
&= \frac{\rho_T}{2} \|\mathbf{v}_h^n\|_{L^2(\Omega^S)}^2 + \mu_S \|\mathbf{D}(\mathbf{d}_h^n)\|_{L^2(\Omega^S)}^2 + \frac{\lambda_S}{2} \|\nabla \cdot \mathbf{d}_h^n\|_{L^2(\Omega^S)}^2 + \frac{\rho_F}{2} \|\mathbf{u}_h^n\|_{L^2(\Omega^F)}^2 \\
&\quad + \frac{\rho_S h}{2} \left(\|\boldsymbol{\xi}_h^n \cdot \boldsymbol{\tau}^S\|_{L^2(\Gamma)}^2 + \|\mathbf{u}_h^n \cdot \mathbf{n}^F\|_{L^2(\Gamma)}^2 \right) \\
&\quad + \frac{1}{2} \|\boldsymbol{\eta}_h^n\|_E^2 + \frac{\Delta t}{2\alpha^f s} \|\mathbf{u}_h^n \cdot \boldsymbol{\tau}^S\|_{L^2(\Gamma)}^2 + \frac{(\Delta t)^2}{2\rho_S h} \|J^n \boldsymbol{\sigma}(\mathbf{u}^n, p^n) \mathbf{n}^F |_{\Gamma} \cdot \mathbf{n}^S\|_{L^2(\Gamma)}^2 \tag{29}
\end{aligned}$$

To make sense of the terms in this estimate we introduce the following notation. First, introduce the kinetic and elastic energy of the discretized coupled problem, respectively:

$$\mathcal{E}_k^n = \frac{\rho_F}{2} \|\mathbf{u}_h^n\|_{L^2(\Omega^F)}^2 + \frac{\rho_T}{2} \|\mathbf{v}_h^n\|_{L^2(\Omega^S)}^2 + \frac{\rho_S h}{2} \left(\|\boldsymbol{\xi}_h^n \cdot \boldsymbol{\tau}^S\|_{L^2(\Gamma)}^2 + \|\mathbf{u}_h^n \cdot \mathbf{n}^F\|_{L^2(\Gamma)}^2 \right), \tag{30}$$

$$\mathcal{E}_e^n = \mu_S \|\mathbf{D}(\mathbf{d}_h^n)\|_{L^2(\Omega^S)}^2 + \frac{\lambda_S}{2} \|\nabla \cdot \mathbf{d}_h^n\|_{L^2(\Omega^S)}^2 + \frac{1}{2} \|\boldsymbol{\eta}_h^n\|_E^2, \tag{31}$$

and denote the total energy of the discretized problem at time t^n by

$$\mathcal{E}^n = \mathcal{E}_k^n + \mathcal{E}_e^n. \tag{32}$$

Next, introduce a discrete analogy of physical dissipation due to fluid viscosity and due to slip between the fluid and thin structure and between the thin and thick structure:

$$\begin{aligned} \mathcal{D}^n = & \Delta t \left(2\mu_F \|\mathbf{D}(\mathbf{u}_h^n)\|_{L^2(\Omega^F)}^2 + \frac{1}{\alpha^{ss}} \|(\mathbf{v}_h^n - \boldsymbol{\xi}_h^n) \cdot \boldsymbol{\tau}^S\|_{L^2(\Gamma)}^2 \right. \\ & \left. + \frac{1}{\alpha^{fs}} \left(\frac{1}{2} \left(\|(\boldsymbol{\xi}_h^n - \mathbf{u}_h^{n-1}) \cdot \boldsymbol{\tau}^S\|_{L^2(\Gamma)}^2 + \|(\mathbf{u}_h^n - \boldsymbol{\xi}_h^n) \cdot \boldsymbol{\tau}^F\|_{L^2(\Gamma)}^2 \right) \right) \right). \end{aligned} \quad (33)$$

Notice how the contribution due to friction in the slip between the fluid and the thin structure, i.e., the two terms in the last line above, is obtained from both the fluid and structure sub-problems, and it contributes to the energy via the average between the two: $\frac{1}{2} \left(\|(\boldsymbol{\xi}_h^n - \mathbf{u}_h^{n-1}) \cdot \boldsymbol{\tau}^S\|_{L^2(\Gamma)}^2 + \|(\mathbf{u}_h^n - \boldsymbol{\xi}_h^n) \cdot \boldsymbol{\tau}^F\|_{L^2(\Gamma)}^2 \right)$.

Finally, we introduce the notation for the terms in the energy equality (29) that are due to *numerical* dissipation. These terms will all tend to zero as $\Delta t \rightarrow 0$:

$$\begin{aligned} \mathcal{E}_{\Delta t}^n &= \frac{\Delta t}{2\alpha^{fs}} \|\mathbf{u}_h^n \cdot \boldsymbol{\tau}^F\|_{L^2(\Gamma)}^2 + \frac{(\Delta t)^2}{2\rho_S h} \|J^n \boldsymbol{\sigma}(\mathbf{u}^n, p^n) \mathbf{n}^F|_{\Gamma} \cdot \mathbf{n}^S\|_{L^2(\Gamma)}^2, \quad (34) \\ \mathcal{D}_{\Delta t}^{n+1,n} &= \frac{\rho_F}{2} \|\mathbf{u}_h^{n+1} - \mathbf{u}_h^n\|_{L^2(\Omega^F)}^2 + \frac{\rho_T}{2} \|\mathbf{v}_h^{n+1} - \mathbf{v}_h^n\|_{L^2(\Omega^S)}^2 + \frac{\rho_s h}{2} \|(\boldsymbol{\xi}_h^{n+1} - \boldsymbol{\xi}_h^n) \cdot \boldsymbol{\tau}^S\|_{L^2(\Gamma)}^2 \\ &+ \mu_S \|\mathbf{D}(\mathbf{d}_h^{n+1} - \mathbf{d}_h^n)\|_{L^2(\Omega^S)}^2 + \frac{\lambda_S}{2} \|\nabla \cdot (\mathbf{d}_h^{n+1} - \mathbf{d}_h^n)\|_{L^2(\Omega^S)}^2 + \frac{1}{2} \|\boldsymbol{\eta}_h^{n+1} - \boldsymbol{\eta}_h^n\|_{\mathbb{E}}^2 \end{aligned} \quad (35)$$

PROPOSITION 1 (Energy Equality) *Let $p_{in/out} = 0$. Then the following energy equality holds:*

$$\mathcal{E}^{n+1} + \mathcal{E}_{\Delta t}^{n+1} + \mathcal{D}^{n+1} + \mathcal{D}_{\Delta t}^{n+1,n} = \mathcal{E}^n + \mathcal{E}_{\Delta t}^n, \quad (36)$$

where \mathcal{E}^n , \mathcal{D}^n , $\mathcal{E}_{\Delta t}^n$, and $\mathcal{D}_{\Delta t}^{n+1,n}$ are defined in (32), (33), and (35).

If we sum all the terms as $n = 0, \dots, N-1$ on both sides, there will be cancellations in all the terms corresponding to \mathcal{E}^{n+1} and $\mathcal{E}_{\Delta t}^{n+1}$ except for the 0-th term corresponding to the initial data, and the N -th term, giving rise to the following estimate:

COROLLARY 1 *Let $p_{in/out} = 0$. Then the following energy inequality holds:*

$$\mathcal{E}^N + \mathcal{E}_{\Delta t}^N \leq \mathcal{E}^0 + \mathcal{E}_{\Delta t}^0. \quad (37)$$

In the continuous case when $\Delta t \rightarrow 0$, the terms due to numerical dissipation in (37) will approach zero since they each contain the factor Δt . This means that estimate (37) approximates well the physical energy of the continuous coupled problem, since it states that the sum of the kinetic and elastic energy is bounded by a constant that depends only on the initial data.

We now consider the case when $p_{in/out}$ is not necessarily equal to zero. The pressure is assumed to be discretized in time by a piecewise constant function so that

$$p_{in/out}(t^n) = \frac{1}{\Delta t} \int_{n\Delta t}^{(n+1)\Delta t} p_{in/out}(t) dt.$$

The non-zero inlet and outlet pressure contribute to the energy estimate via the last term in (26). By replacing the test function with fluid velocity, after using the trace inequality and Korn inequality one obtains the following estimate:

$$|P_{in/out}(t) \int_{\Gamma_{in/out}} u_z| \leq C |p_{in/out}| \|\mathbf{u}\|_{H^1(\Omega^F(t^n))} \leq \frac{C}{2\epsilon} |p_{in/out}|^2 + \frac{\epsilon C}{2} \|\mathbf{D}(\mathbf{u})\|_{L^2(\Omega^F(t^n))}^2.$$

By choosing ϵ such that $\frac{\epsilon C}{2} \leq 2\mu_F$ term on the right is “swallowed” by the viscous term on the left hand-side in the energy equality (29) to obtain:

THEOREM 1 (Energy Inequality) *The following energy inequality holds for the fully discretized problem (25), (26):*

$$\mathcal{E}^{n+1} + \mathcal{E}_{\Delta t}^{n+1} + \mathcal{D}^{n+1} + \mathcal{D}_{\Delta t}^{n+1,n} \leq \mathcal{E}^n + \mathcal{E}_{\Delta t}^n + \Delta t C ((p_{in}^n)^2 + (p_{out}^n)^2), \quad (38)$$

where C is a constant that depends only on the parameters in the problem.

Similarly as before, we can show that this estimate approximates well the continuous energy of the coupled problem by summing both the left and the right hand-sides with respect to $n = 1, \dots, N - 1$, to obtain:

COROLLARY 2 *The following uniform energy estimate hold for the solution of the discretized problem (25), (26):*

$$\mathcal{E}^N + \mathcal{E}_{\Delta t}^N \leq \mathcal{E}^0 + \mathcal{E}_{\Delta t}^0 + \tilde{C} (\|p_{in}^n\|_{L^2(0,T)}^2 + \|p_{out}^n\|_{L^2(0,T)}^2), \quad (39)$$

where constant \tilde{C} only depends on the parameters in the problem.

The pressure terms on the right hand-side were obtained after using Hölder’s inequality from:

$$\Delta t \sum_{n=0}^{N-1} (p_{in}^n)^2 = \Delta t \sum_{n=0}^{N-1} \left(\frac{1}{\Delta t} \int_{n\Delta t}^{(n+1)\Delta t} p_{in}(t) dt \right)^2 \leq \|p_{in}\|_{L^2(0,T)}^2.$$

Again, we see that estimate (39) implies a good discrete approximation of the energy estimate at the continuous level. Estimate (39) implies that as $\Delta t \rightarrow 0$, the kinetic energy and the elastic energy of the coupled problem are uniformly bounded by a constant on the right hand-side, which depends only on the initial data and on the parameters in the problem.

4.3 NUMERICAL RESULTS

Two sets of simulations were performed to test the proposed strategy. One is a fluid-thin structure interaction problem with the Navier slip boundary condition at the fluid-structure interface, and the other is a structure-structure interaction problem with slip at the structure-structure interface.

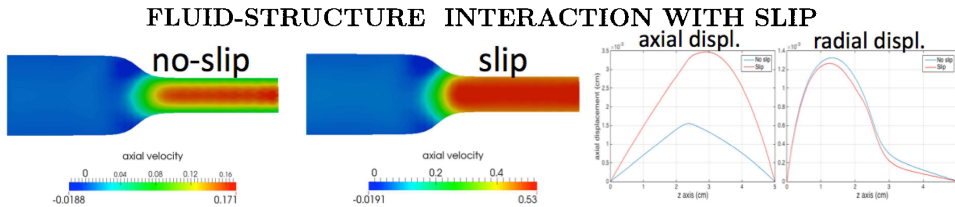


FIGURE 3: Flow through an elastic tube with a throat: slip v.s. no-slip. The two figures on the left show axial velocity. The two figures on the right show displacement: red line corresponds to slip, blue line to no-slip.

Fluid-structure interaction with slip. Motivated by the Ketchup example, we calculated the flow of an incompressible, viscous fluid through an elastic tube with a throat, see Fig. 3, driven by the normal stress inlet/outlet data. The flow is moving from left to right, and it gets faster as it passes through the throat. The fluid domain is moving and a full two-way coupling is considered. By comparing the flow through the throat in both cases we see that the flow with the Navier slip condition (no-stick coating) is significantly faster than the flow when the no-slip condition is used, as expected. One can also see from the colors depicting the axial component of velocity that the velocity profiles are different.

Structure-structure interaction with slip. We considered two structures of finite thickness interacting with each other through a slip condition. See Figs. 4 and 5. Equations of 2D elasticity were used to describe the elastodynamics of each structure. The elasticity properties of both structures were identical. The structures were clamped at the end points and a symmetric, continuous external force (normal stress) was applied at the bottom boundary causing bending, with zero values at the end points, and a maximum value in the middle. Zero normal stress was assigned at the top boundary. The response of the laminated structure with slip was compared to the laminated structure with no-slip (or, equivalently, a single structure with double thickness). The simulations were performed in 2D. Figs. 4 and 5 show the magnitude of displacement, the tangential displacement of the structure-structure interface, and 2D tangential displacement.

We see that the top and bottom structures that are connected via the slip condition stretch in opposite direction at the structure-structure interface while the combined structure bends slightly in the middle. See Figs. 4 right, and 5. The top structure at the interface is stretched from left to right, then in the middle the tangential displacement is zero, and then at the right half the top structure is stretched from right to left. The opposite is true for the bottom structure at the structure-structure interface.

One can clearly see sliding between the two structures in the slip case, which is not present in the no-slip case.

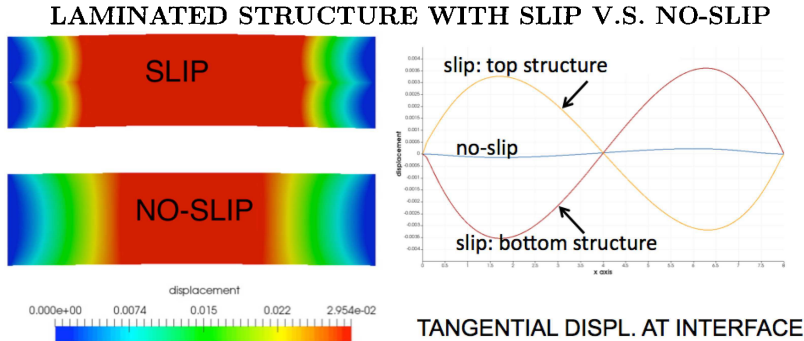


FIGURE 4: Left: **Magnitude of displacement** for laminated structure with a slip (top) and no-slip (bottom) coupling condition. The horizontal interface is in the middle separating two layers. See Fig. 5 for the corresponding 2D tangential displacement. Right: **Tangential displacement at the structure-structure interface**. Positive tangential displacement denotes the motion from left to right, and negative from right to left. The blue line corresponds to the no-slip case, the yellow line corresponds to the tangential interface displacement of the *top* structure slipping over the bottom structure, and the red line corresponds to tangential interface displacement of the *bottom* structure with slip.

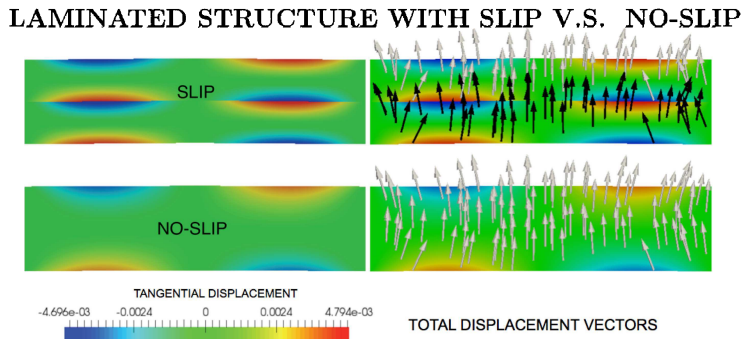


FIGURE 5: The figures show **2D plots of tangential displacement** for laminated structures with slip (top) and no-slip (bottom). Red denotes positive tangential displacement (from left to right) and blue negative (from right to left). The arrows in the two figures on the right show displacement vectors (normalized). One can clearly see sliding between two structures in the slip case, which is not present in the no-slip case.

5 ACKNOWLEDGEMENTS

The authors would like to thank post-doctoral associate Dr. Yifan Wang for the image shown in Figure 1. The work of M. Bukač was supported in part by the National Science Foundation by the grant DMS-1619993. The work by S. Čanić was supported in part by the National Science Foundation by the grants DMS-1318763, DMS-1311709, DMS-1613757, and by the Hugh Roy and Lillie Cranz Cullen Distinguished Professorship funds awarded by the University of Houston. The work of B. Muha was supported in part by the Croatia-USA bilateral grant "Fluid-elastic structure interaction with the Navier slip boundary condition", Croatian Science Foundation grant number 9477.

6 REFERENCES

- [1] Å. Ahlgren, M. Cinthio, S. Steen, H. Persson, T. Sjöberg, and K. Lindström. Effects of adrenaline on longitudinal arterial wall movements and resulting intramural shear strain: a first report. *Clinical physiology and functional imaging*, 29(5):353–359, 2009.
- [2] F. Baaijens. A fictitious domain/mortar element method for fluid-structure interaction. *Int. J. Numer. Meth. Fluids*, 35:743–761, 2001.
- [3] S. Baoukina and S. Mukhin. Bilayer membrane in confined geometry: Interlayer slide and entropic repulsion. *Journal of Experimental and Theoretical Physics*, 99(4):875–888, 2004.
- [4] V. Barbu, Z. Grujić, I. Lasiecka, and A. Tuffaha. Existence of the energy-level weak solutions for a nonlinear fluid-structure interaction model. In *Fluids and waves*, volume 440 of *Contemp. Math.*, pages 55–82. Amer. Math. Soc., Providence, RI, 2007.
- [5] V. Barbu, Z. Grujić, I. Lasiecka, and A. Tuffaha. Smoothness of weak solutions to a nonlinear fluid-structure interaction model. *Indiana Univ. Math. J.*, 57(3):1173–1207, 2008.
- [6] C. Beards and I. Imam. The damping of plate vibration by interfacial slip between layers. *International Journal of Machine Tool Design and Research*, 18:131–137, 1978.
- [7] H. Beirão da Veiga. On the existence of strong solutions to a coupled fluid-structure evolution problem. *J. Math. Fluid Mech.*, 6(1):21–52, 2004.

- [8] M. Bukac and S. Canic. Longitudinal displacement in viscoelastic arteries: a novel fluid-structure interaction computational model, and experimental validation. *Journal of Mathematical Biosciences and Engineering*, 10(2):258–388, 2013.
- [9] M. Bukac, S. Canic, R. Glowinski, B. Muha, and A. Quaini. A modular, operator-splitting scheme for fluid-structure interaction problems with thick structures. *International Journal for Numerical Methods in Fluids*, 74(8):577–604, 2014.
- [10] M. Bukac, S. Canic, R. Glowinski, J. Tambaca, and A. Quaini. Fluid-structure interaction in blood flow capturing non-zero longitudinal structure displacement. *Journal of Computational Physics*, 235(0):515 – 541, 2013.
- [11] M. Bukac, S. Canic, and B. Muha. A partitioned scheme for fluid-composite structure interaction problems. *Journal of Computational Physics*, 281(0):493 – 517, 2015.
- [12] M. Bukac and B. Muha. Stability and convergence analysis of the kinematically coupled scheme for fluid-structure interaction. *SIAM J Num Anal*, 54(5):3032–3061, 2016.
- [13] S. Canic, B. Muha, and M. Bukac. Fluid-structure interaction in hemodynamics: Modeling, analysis, and numerical simulation. In *Fluid-Structure Interaction and Biomedical Applications (Bodnar, Galdi, Necasova eds.)*, Advances in Mathematical Fluid Mechanics. Birkhauser Basel, 2014.
- [14] S. Caniç, B. Muha, and M. Bukač. Stability of the kinematically coupled β -scheme for fluid-structure interaction problems in hemodynamics. *Journal for Numerical Analysis and Modeling*, 12(1):54–80, 2015.
- [15] P. Causin, J. Gerbeau, and F. Nobile. Added-mass effect in the design of partitioned algorithms for fluid-structure problems. *Comput. Methods Appl. Mech. Eng.*, 194(42-44):4506–4527, 2005.
- [16] A. Chambolle, B. Desjardins, M. J. Esteban, and C. Grandmont. Existence of weak solutions for the unsteady interaction of a viscous fluid with an elastic plate. *J. Math. Fluid Mech.*, 7(3):368–404, 2005.
- [17] N. V. Chemetov and Š. Nečasová. The motion of a rigid body in viscous fluid including collisions. A global solvability result. Preprint, 2015.
- [18] C. H. A. Cheng, D. Coutand, and S. Shkoller. Navier-Stokes equations interacting with a nonlinear elastic biofluid shell. *SIAM J. Math. Anal.*, 39(3):742–800 (electronic), 2007.
- [19] C. H. A. Cheng and S. Shkoller. The interaction of the 3D Navier-Stokes equations with a moving nonlinear Koiter elastic shell. *SIAM J. Math. Anal.*, 42(3):1094–1155, 2010.

- [20] M. Cinthio, Å. Ahlgren, J. Bergkvist, T. Jansson, H. Persson, and K. Lindström. Longitudinal movements and resulting shear strain of the arterial wall. *American Journal of Physiology-Heart and Circulatory Physiology*, 291(1):H394–H402, 2006.
- [21] M. Cinthio, A. Ahlgren, T. Jansson, A. Eriksson, H. Persson, and K. Lindstrom. Evaluation of an ultrasonic echo-tracking method for measurements of arterial wall movements in two dimensions. *IEEE transactions on ultrasonics, ferroelectrics, and frequency control*, 52(8):1300–1311, 2005.
- [22] G. Cottet, E. Maitre, and T. Milcent. Eulerian formulation and level set models for incompressible fluid-structure interaction. *Mathematical Modelling and Numerical Analysis*, 42(3):471–492, 2008.
- [23] D. Coutand and S. Shkoller. Motion of an elastic solid inside an incompressible viscous fluid. *Arch. Ration. Mech. Anal.*, 176(1):25–102, 2005.
- [24] D. Coutand and S. Shkoller. The interaction between quasilinear elastodynamics and the Navier-Stokes equations. *Arch. Ration. Mech. Anal.*, 179(3):303–352, 2006.
- [25] J. Donéa. A Taylor-Galerkin method for convective transport problems. In *Numerical methods in laminar and turbulent flow (Seattle, Wash., 1983)*, pages 941–950. Pineridge, Swansea, 1983.
- [26] M. Doyle, S. Tavoularis, and Y. Bougault. *Application of Parallel Processing to the Simulation of Heart Valves*. Springer-Verlag Berlin Heidelberg, 2010.
- [27] K. Falk, N. Fillot, A.-M. Sfarghiu, Y. Berthier, and C. Loison. Interleaflet sliding in lipidic bilayers under shear flow: comparison of the gel and fluid phases using reversed non-equilibrium molecular dynamics simulations. *Physical Chemistry Chemical Physics*, 16(5):2154–2166, 2014.
- [28] L. Fauci and R. Dillon. Biofluidmechanics of reproduction. *Ann. Rev. Fluid Mech.*, 38:371–394, 2006.
- [29] M. A. Fernández. Incremental displacement-correction schemes for the explicit coupling of a thin structure with an incompressible fluid. *C. R. Math. Acad. Sci. Paris*, 349(7-8):473–477, 2011.
- [30] M. A. Fernández. Incremental displacement-correction schemes for incompressible fluid-structure interaction. *Numerische Mathematik*, 123(1):21–65, 2013.
- [31] C. Figueroa, I. Vignon-Clementel, K. Jansen, T. Hughes, and C. Taylor. A coupled momentum method for modeling blood flow in three-dimensional deformable arteries. *Comput. Methods Appl. Mech. Eng.*, 195:5685–5706, 2006.

- [32] D. Gérard-Varet and M. Hillairet. Existence of weak solutions up to collision for viscous fluid-solid systems with slip. *Comm. Pure Appl. Math.*, 67(12):2022–2075, 2014.
- [33] D. Gérard-Varet, M. Hillairet, and C. Wang. The influence of boundary conditions on the contact problem in a 3D Navier-Stokes flow. *J. Math. Pures Appl. (9)*, 103(1):1–38, 2015.
- [34] R. Glowinski. *Finite element methods for incompressible viscous flow*, in: P.G.Ciarlet, J.-L.Lions (Eds), *Handbook of numerical analysis*, volume 9. North-Holland, Amsterdam, 2003.
- [35] C. Grandmont. Existence of weak solutions for the unsteady interaction of a viscous fluid with an elastic plate. *SIAM J. Math. Anal.*, 40(2):716–737, 2008.
- [36] B. Griffith. On the volume conservation of the immersed boundary method. *Commun Comput Phys.*, 12:401–432, 2012.
- [37] B. Griffith, R. Hornung, D. McQueen, and C. Peskin. An adaptive, formally second order accurate version of the immersed boundary method. *J Comput Phys.*, 223:10–49, 2007.
- [38] S. Hansen. Modeling and analysis of multilayer laminated plates. *ESAIM: Proc.: Control and partial differential equations*, 4:117–135, 1998.
- [39] S. Hansen and R. Spies. Structural damping in laminated beams due to interfacial slip. *Journal of Sound and Vibration*, 204:183–202, 1997.
- [40] M. Hillairet. Lack of collision between solid bodies in a 2D incompressible viscous flow. *Comm. Partial Differential Equations*, 32(7-9):1345–1371, 2007.
- [41] M. Hillairet and T. Takahashi. Collisions in three-dimensional fluid structure interaction problems. *SIAM J. Math. Anal.*, 40(6):2451–2477, 2009.
- [42] T. Hughes, W. Liu, and T. Zimmermann. Lagrangian-eulerian finite element formulation for incompressible viscous flows. *Comput. Methods Appl. Mech. Eng.*, 29(3):329–349, 1981.
- [43] M. Ignatova, I. Kukavica, I. Lasiecka, and A. Tuffaha. On well-posedness for a free boundary fluid-structure model. *J. Math. Phys.*, 53(11):115624, 13, 2012.
- [44] M. Krafczyk, J. Tolke, E. Rank, and M. Schulz. Two-dimensional simulation of fluid-structure interaction using lattice-Boltzmann methods. *Comput. Struct.*; 79:2031–2037, 2001.
- [45] I. Kukavica, A. Tuffaha, and M. Ziane. Strong solutions for a fluid structure interaction system. *Adv. Differential Equations*, 15(3-4):231–254, 2010.

- [46] U. Kuttler and W. Wall. Fixed-point fluid-structure interaction solvers with dynamic relaxation. *Computational Mechanics*, 43(1):61–72, 2008.
- [47] J. Lequeurre. Existence of strong solutions to a fluid-structure system. *SIAM J. Math. Anal.*, 43(1):389–410, 2011.
- [48] J. Lequeurre. Existence of Strong Solutions for a System Coupling the Navier–Stokes Equations and a Damped Wave Equation. *J. Math. Fluid Mech.*, 15(2):249–271, 2013.
- [49] A. Mikelić. Rough boundaries and wall laws. *Qualitative properties of solutions to partial differential equations, Lecture notes of Nečas Center for Mathematical Modeling (E. Feireisl, P. Kaplický and J. Mříalek etd.)*, 5:103–134, 2009.
- [50] A. Mikelić, v. Nečasová, and M. Neuss-Radu. Effective slip law for general viscous flows over an oscillating surface. *Mathematical Methods in the Applied Sciences*, 36(15):2086–2100, 2013.
- [51] B. Muha and S. Čanić. Existence of a Weak Solution to a Nonlinear Fluid–Structure Interaction Problem Modeling the Flow of an Incompressible, Viscous Fluid in a Cylinder with Deformable Walls. *Arch. Ration. Mech. Anal.*, 207(3):919–968, 2013.
- [52] B. Muha and S. Canic. A nonlinear, 3d fluid-structure interaction problem driven by the time-dependent dynamic pressure data: a constructive existence proof. *Communications in Information and Systems*, 13(3):357–397, 2013.
- [53] B. Muha and S. Canic. Existence of a solution to a fluid–multi-layered-structure interaction problem. *J. Differential Equations*, 256(2):658–706, 2014.
- [54] B. Muha and S. Canic. Fluid-structure interaction between an incompressible, viscous 3D fluid and an elastic shell with nonlinear Koiter membrane energy. *Interfaces and free boundaries*, 17(4):465–495, 2015.
- [55] B. Muha and Z. Tutek. Note on evolutionary free piston problem for Stokes equations with slip boundary conditions. *Commun. Pure Appl. Anal.*, 13(4):1629–1639, 2014.
- [56] B. Muha and S. Čanić. Existence of a weak solution to a fluid-structure interaction problem with the navier slip boundary condition. *Journal of Differential Equations*, 260(12):8550–8589, 2016.
- [57] C. Navier. Sur les lois de léquilibre et du mouvement des corps elastiques. *Mem. Acad. R. Sci. Inst. France*, 369, 1827.
- [58] J. Neustupa and P. Penel. A weak solvability of the Navier-Stokes equation with Navier’s boundary condition around a ball striking the wall. In *Advances in mathematical fluid mechanics*, pages 385–407. Springer, Berlin, 2010.

- [59] Z. Peng, R. Asaro, and Q. Zhu. Multiscale modelling of erythrocytes in stokes flow. *Journal of Fluid Mechanics*, 686:299–337, 2011.
- [60] Z. Peng, X. Li, I. Pivkin, M. Dao, G. Karniadakis, and S. Suresh. Lipid bilayer and cytoskeletal interactions in a red blood cell. *Proceedings of the National Academy of Sciences*, 110(33):13356–13361, 2013.
- [61] C. Peskin. Numerical analysis of blood flow in the heart. *J. Comput. Phys.*, 25:220–252, 1977.
- [62] C. Peskin and D. McQueen. A three-dimensional computational method for blood flow in the heart i. immersed elastic fibers in a viscous incompressible fluid. *J. Comput. Phys.*, 81(2):372–405, 1989.
- [63] G. Planas and F. Sueur. On the “viscous incompressible fluid + rigid body” system with Navier conditions. *Ann. Inst. H. Poincaré Anal. Non Linéaire*, 31(1):55–80, 2014.
- [64] M. Potomkin, V. Gyrya, I. Aranson, and L. Berlyand. Collision of microswimmers in viscous fluid. *Physical Review E*, 87:053005, 2013.
- [65] A. Quarteroni and A. Tuveri, M. andVeneziani. Computational vascular fluid dynamics: problems, models and methods. survey article. *Comput. Visual. Sci.*, 2:163–197, 2000.
- [66] J.-P. Raymond and M. Vanninathan. A fluid–structure model coupling the Navier-Stokes equations and the lamé system. *Journal de Mathématiques Pures et Appliqués*, 102(3):546–596, 2012.
- [67] J. A. San Martín, V. Starovoitov, and M. Tucsnak. Global weak solutions for the two-dimensional motion of several rigid bodies in an incompressible viscous fluid. *Arch. Ration. Mech. Anal.*, 161(2):113–147, 2002.
- [68] S. Srinivasan, W. Choi, K. Park, S. Chhatre, R. Cohen, and G. McKinley. Drag reduction for viscous laminar flow on spray-coated non-wetting surfaces. *Soft Matter*, 9:5691–5702, 2013.
- [69] C. Wang. Strong solutions for the fluid-solid systems in a 2-D domain. *Asymptot. Anal.*, 89(3-4):263–306, 2014.
- [70] J. Williams. Developments in composite structures for the offshore oil industry. *Offshore Technology Conference, Houston*, May, 1990.
- [71] A. Yeung and E. Evans. Unexpected dynamics in shape fluctuations of bilayer vesicles. *Journal de Physique II*, 5(10):1501–1523, 1995.